

Negative-Mass Effects in Spin-Orbit Coupled Bose-Einstein Condensates

David Colas,^{1,*} Fabrice P. Laussy,^{2,3} and Matthew J. Davis¹

¹*ARC Centre of Excellence in Future Low-Energy Electronics Technologies, School of Mathematics and Physics, University of Queensland, St Lucia, Queensland 4072, Australia*

²*Faculty of Science and Engineering, University of Wolverhampton, Wulfruna Street, Wolverhampton WV1 1LY, United Kingdom*

³*Russian Quantum Center, Novaya 100, 143025 Skolkovo, Moscow Region, Russia*

 (Received 27 December 2017; revised manuscript received 9 June 2018; published 31 July 2018)

Negative effective masses can be realized by engineering the dispersion relation of a variety of quantum systems. A recent experiment with spin-orbit coupled Bose-Einstein condensates has shown that a negative effective mass can halt the free expansion of the condensate and lead to fringes in the density [M. A. Khomehchi *et al.*, *Phys. Rev. Lett.* **118**, 155301 (2017)]. Here, we show that the underlying cause of these observations is the self-interference of the wave packet that arises when only one of the two effective mass parameters that characterize the dispersion of the system is negative. We show that spin-orbit coupled Bose-Einstein condensates may access regimes where both mass parameters controlling the propagation and diffusion of the condensate are negative, which leads to the novel phenomenon of counterpropagating self-interfering packets.

DOI: [10.1103/PhysRevLett.121.055302](https://doi.org/10.1103/PhysRevLett.121.055302)

The most straightforward definition of mass in classical physics is expressed by Newton's second law. The acceleration \mathbf{a} of an object is related to the net force \mathbf{F} acting upon it, with the mass m being the proportionality constant: $\mathbf{F} = m\mathbf{a}$. In this context, a particle with a negative mass would behave strangely by accelerating in the opposite direction of an applied force. This cannot happen in free space, but the concept of mass can be extended beyond this simple scenario. In solid-state physics, an *effective* mass was originally introduced to describe the motion of electrons in the periodic potential induced by crystal lattices [1]. The effective mass m^* is related to the curvature of the dispersion relation, and for many quasiparticles, this is nonparabolic, leading to a mass that depends on the wave vector. A negative m^* can occur, e.g., for semiconductor holes near the top of a valence band.

A more general definition of mass is required when we consider both the propagation and diffusion of wave packets. The dispersion can be expanded in a Taylor series around k_0 as $E(k) \approx E_0 + \hbar^2 k_0(k - k_0)/m_1(k_0) + \hbar^2(k - k_0)^2/[2m_2(k_0)] + \dots$, and the coefficients of each order term relate to a new mass parameter that has certain characteristic effects on the dynamics [2,3]. We define

$$m_1(k) = \hbar^2 k [\partial_k E(k)]^{-1}, \quad (1)$$

$$m_2(k) \equiv m^* = \hbar^2 [\partial_k^2 E(k)]^{-1}. \quad (2)$$

The parameter m_1 is related to the classical motion of the wave packet via the group velocity $v_g = \hbar k/m_1$. The parameter m_2 determines the acceleration of the packet

when an external force is applied, as well as its rate of diffusion [4]. For a purely parabolic dispersion, we would find that $m_1 = m_2$, but in other systems, m_1 and m_2 can have different signs, be zero, or even become infinite.

A number of experimental platforms in physics now allow dispersion engineering. For example, exciton-polaritons produced in semiconductor microcavities [5] have a nonparabolic dispersion that can be controlled by detuning the cavity and the exciton modes, leading to a variety of exotic effects [6–8]. Recent theoretical and experimental studies have shown that polariton wave packets can exhibit a counterintuitive flow resulting from a divergence of the effective mass m_2 , in the form of self-interfering packets (SIP) [4], backflow [9], and superluminal X waves [10]. When the wave packet spreads over this singularity of the mass, it straddles regions of positive and negative effective mass, effectively bouncing the packet back onto itself and producing self-interference.

Another system that allows for the control of the dispersion of wave packets is an atomic Bose-Einstein condensate (BEC). Early experiments demonstrated dispersion engineering by loading a condensate into a weak optical lattice [11–13]. Bright solitons were subsequently realized in repulsive atomic and polariton BECs by loading them into a quasimomentum state with negative m_2 to counterbalance the effect of repulsive interactions [13,14]. More recently, artificial spin-orbit interactions in two-component BECs have allowed the engineering of more complex dispersions through the control of the Raman laser setup [15–17]. Interestingly, this allows the possibility of generating negative regions for both m_1 and

m_2 , which is not straightforward to achieve in polariton systems. In recent work, Khamsehchi *et al.* have shown how the peculiar dispersion relation of an atomic spin-orbit coupled Bose-Einstein condensate (SOCBEC) can indeed lead to unconventional wave packet dynamics, interpreted as “negative-mass hydrodynamics,” and reported phenomena such as self-trapping, soliton trains, and dynamical instabilities [18].

In this Letter, we clarify the role of the two effective mass parameters m_1 and m_2 in determining the condensate dynamics in the SOCBEC platform. In particular, we show that the experimental observation of inhibited expansion by Khamsehchi *et al.* [18] arises from a negative m_2 parameter and leads to the linear SIP phenomenon predicted earlier for exciton-polariton BEC [4]. In the experiment, the nonlinearity of the condensate then causes the interference fringes from the SIP to transform into solitons. We further show that a negative m_1 parameter can also be achieved in SOCBECs and would lead to the more striking phenomenology of a wave packet moving in the opposite direction of its momentum. In particular, we investigate the dynamics in a regime where both m_1 and m_2 are negative, which leads to the condensate splitting into two counter-propagating SIPs. This is within reach of the current experimental platforms by simply tuning the Raman parameters. A clear understanding of the underlying mechanics of the wave packet dynamics can be obtained by performing its wavelet decomposition. Our work thus provides a comprehensive understanding of the effect of negative masses in SOCBECs.

We consider an identical spin-orbit coupling setup to Khamsehchi *et al.* [18], with a ^{87}Rb BEC for which two internal $5S_{1/2}$ spin states are isolated, leading to the so-called hyperfine pseudospin-up and pseudospin-down states [15]: $|\uparrow\rangle = |F=1, m_F=0\rangle$ and $|\downarrow\rangle = |F=1, m_F=-1\rangle$. Two Raman lasers are used to couple the two states with a strength Ω and detuned by $\delta/2$ from the Raman resonance, as shown in Fig. 1(a). The system dynamics is described in units of energy and momentum defined by the recoil energy $E_R = (\hbar k_R)^2/2m$ and Raman wave vector $k_R = 2\pi/\sqrt{2}\lambda_R$, where λ_R is the Raman wavelength. For a homogeneous and noninteracting gas, the system is described by the k -space Hamiltonian [15],

$$H = \begin{pmatrix} \frac{\hbar k(k+2k_R)}{2m} + \frac{\delta}{2} & \frac{\Omega}{2} \\ \frac{\Omega}{2} & \frac{\hbar k(k-2k_R)}{2m} - \frac{\delta}{2} \end{pmatrix}, \quad (3)$$

which acts on the spinor field $\psi = (\psi_\uparrow, \psi_\downarrow)^T$. Diagonalizing the Hamiltonian mixes the spin states and leads to upper (+) and lower (−) energy bands,

$$E_\pm(k) = \frac{\hbar k^2}{2m} \pm \sqrt{\left(\gamma k + \frac{\delta}{2}\right)^2 + \left(\frac{\Omega}{2}\right)^2}, \quad (4)$$

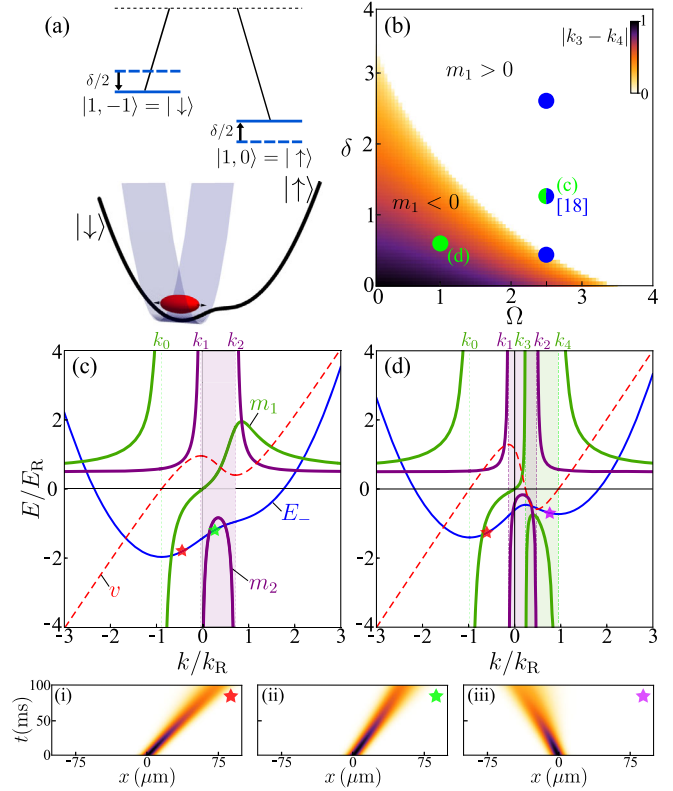


FIG. 1. (a) Schematic of the experimental configuration. The BEC initially resides at the bottom of the lower branch shaped by the spin-orbit coupling (see energy level diagram). The trap is then released in the x dimension to let the BEC expand. (b) Parameter space for m_1 , defined by the momentum range $|k_3 - k_4|$ for which m_1 is negative. Blue dots: configurations considered in [18]. Green dots: configurations explored here. (c) SOCBEC dispersion properties for $\Omega = 2.5$, $\delta = 1.36$, $k_R = 1$ (from Ref. [18]). Blue line: lower branch E_- . Green line: effective mass m_1 . Purple line: effective mass m_2 . Red dashed line: group velocity v . The lower branch presents a region with $m_2 < 0$, where v decreases with increasing k . (d) As for (c), but $\Omega = 1$, $\delta = 0.7$, $k_R = 1$, E_- has regions with both $m_1 < 0$ and $m_2 < 0$, and v has an opposite sign to the momentum. (i–iii) Examples of wave packet propagation, the colored stars indicate where E_- is excited.

where $\gamma = \hbar k_R/m$. The dispersion relation for the lower band for two sets of Raman laser parameters k_R , Ω , and δ , are shown as a blue line in Figs. 1(c) and 1(d). As both are clearly nonparabolic, it is important to consider both the first and second mass parameters, rather than only m_2 that was discussed in Ref. [18]. The parameter space for m_1 is plotted in Fig. 1(b), where we have identified the sets of parameters considered in Ref. [18] as well as those of the present Letter. We emphasize that the dispersion relation in Fig. 1(c) is identical to one set of SOC parameters considered in Ref. [18].

We now focus on the properties of the lower branch. An inflection point of this branch corresponds to a change of sign of m_2 , which becomes infinite at the points $k_{1,2}$

meaning that wave packets with this quasimomentum do not diffuse [19]. Similarly, one can define the points $k_{0,3,4}$ at which the mass m_1 diverges [19]. Most of the dynamics can now be understood regarding only the k -dependent group velocity $v(k)$, directly shaped by m_1 and m_2 [19]. As can be seen in Figs. 1(c) and 1(d), the linear parts of the dispersion, when m_2 diverges at $k_{1,2}$, lead to a local minimum or maximum for the group velocity. Similarly, v is zero when the dispersion is locally flat at the points $k_{0,3,4}$ and takes negative values between k_3 and k_4 , where $m_1 < 0$. A negative m_1 here corresponds to the packet moving in the opposite direction to the applied impulse, thus reversing the sign of the group velocity. We show in Figs. 1(i)–(iii) typical examples of wave packet propagation when exciting the branch at different quasimomenta.

For the dispersion shown in Fig. 1(c), consider applying an impulse to move from the red (i) to the green (ii) star, where $m_2 < 0$. The wave packet decelerates but keeps propagating in the same direction. Conversely, for the dispersion shown in Fig. 1(d), applying an impulse to move from the red (i) to the purple star (iii) (where $v < 0$), one sees that the wave packet not only slows down but actually reverses direction. We have provided an online interactive plot of the dispersion as a function of its key parameters δ , Ω , and k_R [20].

We now analyze one-dimensional simulations of the dynamics of SOCBEC expansion in the context of m_1 and m_2 using the experimental parameters for $\delta = 1.36$ and $\Omega = 2.5$ from Ref. [18,21]. The dynamics of a 1D BEC initially positioned at the bottom of the lower branch and released from a harmonic trap in one direction can be described by a single-band Gross-Pitaevskii equation:

$$i\partial_t\psi(x) = \mathcal{F}_x^{-1}[E_-(k)\psi(k)] + g|\psi(x)|^2\psi(x), \quad (5)$$

where $E_-(k)$ is the lower branch dispersion derived in Eq. (4) and shown in Fig. 1(c), \mathcal{F}_x^{-1} is the inverse Fourier transform, and g the effective 1D interaction strength.

We initially focus on the linear dynamics by setting $g=0$ so that we can study the free wave packet propagation with this dispersion, for which only m_2 is negative. We begin with a narrow Gaussian wave packet ($\sigma_x = 0.25 \mu\text{m}$) centered at the minimum of the branch, so that its momentum spread encompasses the range k_1-k_2 [22]. The spacetime evolution of the wave function $|\psi(x,t)|^2$ is plotted in Fig. 2(a) and shows a distinct interference pattern spatially confined in the diffusion cone defined by $d_{1,2}(t) = v(k=k_{1,2})t$. An enlightening method to visualize the self-interference effect is to plot the wave function density in the x - k plane by performing the wavelet transform (WT) $\mathbb{W}(x,k) = (1/\sqrt{|k|}) \int_{-\infty}^{\infty} \psi(x)\mathcal{G}^*[(x-x_0)/k]dx$ [23]. Recent studies have shown that the WT can be applied to analyse complex interacting wave packets dynamics [4,24]. Unlike the usual Fourier transform based on the decomposition of the signal into a sum of delocalised

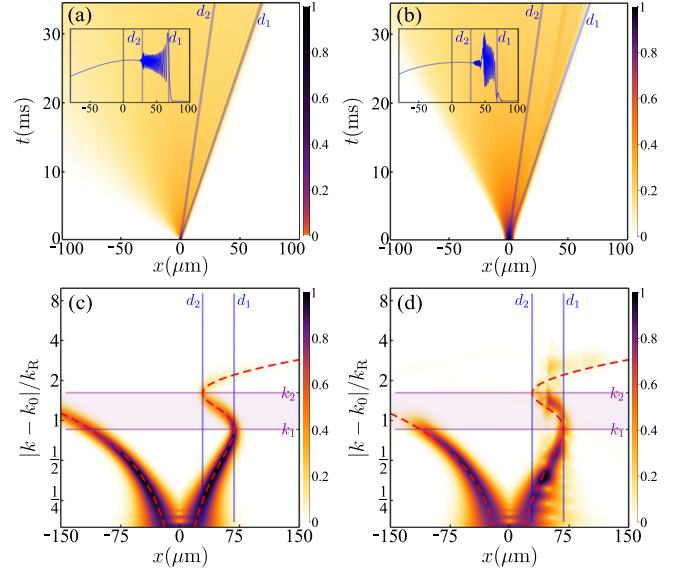


FIG. 2. BEC expansion with the SOC dispersion of Fig. 1(c). The first column shows the linear case with $g = 0$ and the second column the interacting case. (a,b) Spacetime evolution of $|\psi(x,t)|^2$, with a condensate initial size of (a) $0.25 \mu\text{m}$ and (b) $5 \mu\text{m}$ Thomas-Fermi radius, obtained from the ground state of a 10^4 particles BEC released from a 100 Hz trap. Insets: density at $t = 35$ ms. (c,d) Wavelet decomposition of $\psi(x)$ at $t = 35$ ms. Vertical blue lines: limits of the diffusion cone in x . Purple horizontal lines: position of the inflection points in k . Red dashed curve: classical displacement $d(k)$ of each k -wave vector. An animation (video S1) of this figure is provided in the Supplemental Material [19].

functions (sine and cosine), the WT uses localised wavelets. Here we choose the Gabor wavelet family, with Gaussian-like functions \mathcal{G}^* , and a high central frequency ensuring good resolution near the inflection points in the dispersion [25]. Further details regarding the WT for wave packets are described in the Supplemental Material [19].

Figure 2(c) shows the wavelet energy density $|\mathbb{W}(x,k)|^2$ at $t = 35$ ms. The inflection point momenta $k_{1,2}$ are indicated in k (purple lines), and the boundaries $d_{1,2}$ of the diffusion cone in x (blue lines). We also plot the displacement $d(k) = v(k)t$ associated with each k -wave vector (red dashed line). From this simple picture, one can now understand the origin of the self-interference effect: different wave vectors of the packet travel with the same velocity, hence overlapping in real space and interfering. This happens only when the wave packet spreads over an inflection point of the branch. This phenomenology is a universal consequence of the shape of the dispersion and can therefore be equally encountered for exciton-polariton and atomic condensates, despite their operating timescales that differ by nine orders of magnitude.

Practically, it is challenging to form a SOCBEC with such a broad spread in momentum. One way to overcome this difficulty is to load the packet directly in the inflection

points region by imparting it with the appropriate momentum. A second way, used in the experiment of Khamsehchi *et al.* [18], is to release the BEC from the trap leading to a broadening of the wave packet in k space due to the conversion of interaction energy to kinetic energy. This is an effective way to push some components of the wave packet into the negative m_2 region. Further details of this approach are presented in the Supplemental Material [19].

Here, we simulate the expansion dynamics of an interacting system initially in a 100 Hz harmonic trap with a Thomas-Fermi radius of $5 \mu\text{m}$ corresponding to approximately 10^4 atoms. This is more tightly confined with fewer atoms than the experiment of Ref. [18], which had a trap frequency of 26 Hz, 10^5 atoms, and a Thomas-Fermi radius of $23 \mu\text{m}$, but enables a direct comparison with the $g = 0$ case. The results for the spacetime density and WT are shown in Figs. 2(b) and 2(d). Here, the interference only becomes visible after a finite time, which is that needed for the expansion of the wave packet to reach k_1 . The presence of self-interference is again confirmed by the WT analysis in Fig. 2(d). Because of the interactions, the self-interference pattern differs slightly from the noninteracting case, and the energy density distribution gets spread around $d(k)$ since this curve accounts for the packet's k -components displacement from $t = 0$. The initial packet is here 20 times larger, and only the low k region is significantly populated at $t = 0$. We provide analysis of the exact experimental situation of Khamsehchi *et al.* [18] in the Supplemental Material [19]. Their configuration has a larger nonlinearity which results in the population of k components above k_2 , which travel with a velocity larger than $v(k_1)$. This results in the density “leaking out” of the diffusion cone (d_1) and was previously identified as being due to dynamical instability [18]. The limited diffusion of the condensate as shown in Fig. 2(b), which might appear as a “self-trapping” effect, can be overcome if high enough momenta ($k > k_2$) are reached, as is the case in Ref. [18].

We now study the SOCBEC dispersion in a more interesting configuration that exhibits a stronger type of negative mass effect, shown in Fig. 1(d). This can be obtained by reducing the Raman coupling Ω and detuning δ . In this case, the mass m_1 is also negative in the momentum range k_3-k_4 for which $v < 0$. Again, we first consider the noninteracting case ($g = 0$) but this time with a Gaussian packet centered on $k = k_2$ with a width $\sigma_x = 0.25 \mu\text{m}$. As shown in Fig. 3(a), the wave packet exhibits a double SIP effect during its propagation as the initial state spreads over both k_1 and k_2 . The most notable feature is the position of the second SIP, whose diffusion is limited by $d_2 = v(k_2)t$ in the $x < 0$ region, as $k_3 < k_2 < k_4$. The packet is now composed of two subpackets, each carrying and propagating a SIP in opposite directions. This can be seen in the WT in Fig. 3(c), where we have added the boundaries $k_{3,4}$ (green lines) delimiting the $m_1 < 0$ region. One can see how the wavelet energy density in the

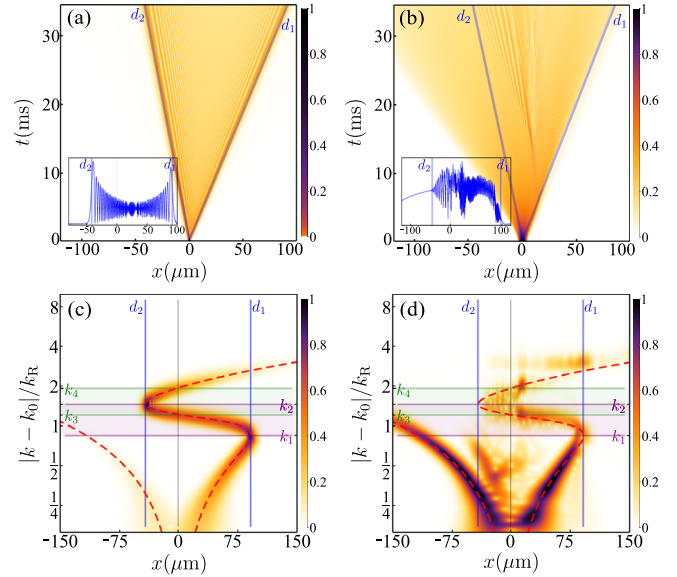


FIG. 3. BEC expansion with the SOC dispersion of Fig. 1(d) with both $m_1 < 0$ and $m_2 < 0$. The first column shows the noninteracting case with $g = 0$ and the second column the interacting case. (a,b) Spacetime evolution of $|\psi(x, t)|^2$, with a condensate initial size of (a) $0.25 \mu\text{m}$ and (b) $5 \mu\text{m}$ Thomas-Fermi radius, obtained from the ground state of a $\approx 2.5 \times 10^4$ particles BEC released from a 100 Hz trap. Insets: density at $t = 35$ ms. (c,d) Wavelet decomposition of $\psi(x)$ at $t = 35$ ms. The color code is the same as Figs. 2(c) and 2(d) with additional horizontal green lines delimiting the $m_1 < 0$ region. An animation (video S2) of this figure is provided in the Supplemental Material [19].

momentum range k_3-k_4 is only displayed in the $x < 0$ region. This corresponds to the packet's k components experiencing backward propagation.

The double SIP behavior can also be observed in the expansion of an interacting BEC. We again begin with the condensate ground state in a 100 Hz trap with a Thomas-Fermi radius of $6 \mu\text{m}$, corresponding to $\approx 2.5 \times 10^4$ atoms, leading to the population of higher momenta as compared to the previous case. As before, the SIP effect is present within the overall diffusing packet as can be seen in Fig. 3(b), and in the WT shown in Fig. 3(d), one can see that the SIP is “delayed” as compared to the noninteracting case. Time-animated videos of $|\psi(x, t)|^2$ with $|\mathbb{W}(x, k)|^2$ for both the linear and interacting cases as presented in Figs. 2 and 3 are provided in Ref. [19]. In experiments, translating optical lattices or Bragg pulses could be used to impart a momentum to the condensate in order to more clearly exhibit the SIP effect [17]. Other nonlinear features like shock waves or soliton trains observed by Khamsehchi *et al.* [18] may appear *a posteriori* as the self-interference process induces large oscillations of the condensate density and thus provide a breeding ground for these excitations. In this experiment, both these linear and nonlinear effects are intertwined and cannot be clearly

separated in the dynamics. The limited diffusion of the condensate, sometimes described as a nonlinear self-trapping effect in the literature [26–28], can instead be viewed in this case as a consequence of peculiar dispersion relations containing inflection points and regions of negative effective mass. Although the condensate diffusion is strongly affected, it is not bounded, and normal diffusion can still occur as the dispersion returns to being parabolic at higher momenta.

In conclusion, we have shown that SOCBECS provide an excellent platform to engineer dispersion relations, allowing the creation of regions of negative effective mass for both parameters m_1 and m_2 that govern wave packet dynamics. The mass m_1 leads to a negative group velocity for a positive impulse, while the mass m_2 leads to self-interference in the wave packet. Self-interference alone is a direct consequence of the linear dynamics where dispersion relations contain inflection points. The nonlinearity of the BEC can further add to the phenomenology, in particular, by populating such regions in the momentum space and allowing self-interference to subsequently lead to the formation of solitons. The wave packet dynamics for which both mass parameters are negative is within reach of the SOCBECS platforms. This would result in the formidable phenomenology of moving an object in the direction opposite to which it was pushed.

This research was supported by the Australian Research Council Centre of Excellence in Future Low-Energy Electronics Technologies (Project No. CE170100039) and funded by the Australian Government. It was also supported by the Ministry of Science and Education of the Russian Federation through the Russian-Greek Project No. RFMEFI61617X0085 and the Spanish MINECO under Contract No. FIS2015-64951-R (CLAUQUE).

*d.colas@uq.edu.au

- [1] C. Kittel, *Introduction to Solid State Physics*, 8th ed. (Wiley, New York, 2004).
- [2] J. Larson, J. Salo, and S. Stenholm, *Phys. Rev. A* **72**, 013814 (2005).
- [3] O. A. Egorov, D. V. Skryabin, A. V. Yulin, and F. Lederer, *Phys. Rev. Lett.* **102**, 153904 (2009).
- [4] D. Colas and F. P. Laussy, *Phys. Rev. Lett.* **116**, 026401 (2016).
- [5] A. Kavokin, J. J. Baumberg, G. Malpuech, and F. P. Laussy, *Microcavities*, 2nd ed. (Oxford University Press, Oxford, 2017).
- [6] P. G. Savvidis, J. J. Baumberg, R. M. Stevenson, M. S. Skolnick, D. M. Whittaker, and J. S. Roberts, *Phys. Rev. Lett.* **84**, 1547 (2000).
- [7] A. Amo, D. Sanvitto, F. P. Laussy, D. Ballarini, E. del Valle, M. D. Martin, A. Lemaître, J. Bloch, D. N. Krizhanovskii, M. S. Skolnick *et al.*, *Nature (London)* **457**, 291 (2009).
- [8] G. Tosi, F. M. Marchetti, D. Sanvitto, C. Antón, M. H. Szymańska, A. Berceanu, C. Tejedor, L. Marrucci, A. Lemaître, J. Bloch *et al.*, *Phys. Rev. Lett.* **107**, 036401 (2011).
- [9] D. Ballarini, D. Caputo, C. S. Muñoz, M. D. Giorgi, L. Dominici, M. H. Szymańska, K. West, L. N. Pfeiffer, G. Gigli, F. P. Laussy *et al.*, *Phys. Rev. Lett.* **118**, 215301 (2017).
- [10] A. Gianfrate, L. Dominici, O. Voronych, M. Matuszewski, M. Stobińska, D. Ballarini, M. D. Giorgi, G. Gigli, and D. Sanvitto, *Light Sci. Appl.* **7**, 17119 (2018).
- [11] B. Eiermann, P. Treutlein, T. Anker, M. Albiez, M. Taglieber, K.-P. Marzlin, and M. K. Oberthaler, *Phys. Rev. Lett.* **91**, 060402 (2003).
- [12] O. Morsch and M. Oberthaler, *Rev. Mod. Phys.* **78**, 179 (2006).
- [13] B. Eiermann, T. Anker, M. Albiez, M. Taglieber, P. Treutlein, K.-P. Marzlin, and M. K. Oberthaler, *Phys. Rev. Lett.* **92**, 230401 (2004).
- [14] M. Sich, D. Krizhanovskii, M. Skolnick, A. Gorbach, R. Hartley, D. V. Skryabin, E. A. Cerda-Méndez, K. Biermann, R. Hey, and P. Santos, *Nat. Photonics* **6**, 50 (2012).
- [15] Y. J. Lin, K. Jimenez-Garcia, and I. B. Spielman, *Nature (London)* **471**, 83 (2011).
- [16] Y. Zhang, L. Mao, and C. Zhang, *Phys. Rev. Lett.* **108**, 035302 (2012).
- [17] C. Hamner, Y. Zhang, M. A. Khamehchi, M. J. Davis, and P. Engels, *Phys. Rev. Lett.* **114**, 070401 (2015).
- [18] M. A. Khamehchi, K. Hossain, M. E. Mossman, Y. Zhang, T. Busch, M. M. Forbes, and P. Engels, *Phys. Rev. Lett.* **118**, 155301 (2017).
- [19] See Supplemental Material at <http://link.aps.org/supplemental/10.1103/PhysRevLett.121.055302> for a detailed analysis on the dispersion properties, details on the wavelet transform applied to wave packets, a further description of the expansion of the BEC that broadens the momentum space wave packet, the comparison with the experimental case, and a description of videos S1, S2 and S3.
- [20] <http://demonstrations.wolfram.com/DispersionPropertiesOfASpinOrbitCoupledBoseEinsteinCondensat/>.
- [21] We note that Ref. [18] showed that simulations of the 1D and 3D Gross-Pitaevskii equations gave quantitatively similar results.
- [22] For ^{87}Rb , this width would require a harmonic trap of frequency 1860 Hz for $g = 0$.
- [23] L. Debnath and F. A. Shah, *Wavelet Transforms and Their Applications*, 2nd ed. (Birkhäuser, Basel, 2015).
- [24] C. H. Baker, D. A. Jordan, and P. M. Norris, *Phys. Rev. B* **86**, 104306 (2012).
- [25] G. I. Márk, *Eur. Phys. J. B* **18**, 247 (1997).
- [26] T. Anker, M. Albiez, R. Gati, S. Hunsmann, B. Eiermann, A. Trombettoni, and M. K. Oberthaler, *Phys. Rev. Lett.* **94**, 020403 (2005).
- [27] T. J. Alexander, E. A. Ostrovskaya, and Y. S. Kivshar, *Phys. Rev. Lett.* **96**, 040401 (2006).
- [28] J. K. Xue, A. X. Zhang, and J. Liu, *Phys. Rev. A* **77**, 013602 (2008).